A comprehensive study on the thermodynamics of the $Al_{13}Fe_4$ solid solution in the Al-Fe-Mn ternary system.

Paul Lafaye[a,*], Kentaro Oishi[a], J-P Harvey[a]

[a] *CRCT- Polytechnique Montréal, Chem. Eng., Box 6079, Station Downtown, Montréal, Qc, Canada, H3C 3A7*

Abstract

This paper presents investigations on the thermodynamic stability of the $Al_{13}Fe_4$ solid solution in the Al-Fe-Mn ternary system as well as its crystal chemistry characterisation. In order to carry out this study, the isobaric heat capacity of the solution was measured at high temperature using a high precision three-dimensional probe. The heat capacity of the $Al_{13}Fe_4$ binary compound measured in this study between 600 K and 1223 K is $C_P(T) = 23.97 + 8.18.10^{-2}T - 7.63.10^5T^2$. This value is significantly different from other measurements reported in the literature. We show in this paper that our measurements are more accurate than those available in the literature thanks to the use of a more precise sensor (3D-Cp sensor versus planar DSC sensor). As a result, our measurements are more thermodynamically consistent with the enthalpy of formation values of the $Al_{13}Fe_4$ compound available in the literature, as well as with our own enthalpy of formation measurement performed independently of the heat capacity measurement presented in this paper. Measurements of the enthalpy of formation of the solid solution were also performed by $in - situ$ synthesis in a DSC. These new measurements were complemented by DFT calculations of the enthalpy of formation at 0 K of the solid solution. Our calculations and measurements show that the substitution of Fe by Mn is responsible for a large increase in the solid solution enthalpy of formation. These new experimental and calculated data were used to develop a thermodynamic model of the solution. Finally, we utilized our model to calculate the Fe site occupation factors (sof) of the solid solution structure over its entire chemical composition range (simulating the complete substitution of all Fe atoms with Mn) as a function of temperature. The chemical ordering of the solid solution was thus quantified, revealing its ideal nature near its melting temperature. These results allowed the development of a new SL-model for the solution, both simpler and more reliable than those used in the literature.

*Corresponding author, email address: paul.lafaye@polymtl.ca

1. Introduction

Ternary solid solutions of the $Al_{13}Fe_4$ compound (space group $C2/m$) have recently received renewed interest from the scientific community [1, 2, 3, 4]. These solutions have been found to play a key role in the fine tuning of both mechanical and corrosion resistance properties of aluminium alloys over unusually high temperature ranges [4, 5, 6, 7, 8]. Moreover, the addition of certain elements to the $Al_{13}Fe_4$ compound such as Pt has led to the development of new environmentally friendly catalysts for hydrogenation reactions [9]. From a more fundamental point of view, the $Al_{13}Fe_4$ structure has been particularly studied by crystallographers as an approximant of quasicrystals [10, 11]. At last, let us note that solid solutions of $Al_{13}Fe_4$ compound are common by-products of the synthesis of Al-based magnetocaloric materials [12, 13].

$Al_{13}Fe_4$-based solid solutions can originate from the substitution of Fe atoms (by Co [4, 14], Cr [4, 15], Ni [4, 16, 17], Pt [9, 18]) or the substitution of Al atoms (by Ta [19], Ti [20], Si [3], Zn [21]). As mentioned in our previous paper dedicated to the $Al_{13}Fe_4$-based solid solutions [22], the solutions resulting from the substitution of Fe atom exhibit generally, but not always, a wider homogeneity range than those resulting from Al atom substitution, with in particular the case of a complete solid solution in the Al-Fe-Co ternary system.

In the Al-Fe-Mn ternary system, the $Al_{13}Fe_4$ solid solution is stable over a wide homogeneity range [23]. The solid solution presents a homogeneity range extending along the $Al_{13}Fe_4$-$Al_{13}Mn_4$ iso-composition line, suggesting a prevalent substitution of Mn on the Fe sites. At a temperature of 1293 K, the maximum Mn content in the solution is 9.5 at.% which corresponds to about 40% of the Fe atoms substituted by Mn. Despite this relatively large homogeneity range, site occupancy data are not available for the $Al_{13}Fe_4$ solid solution in the Al-Fe-Mn system but are essential to design a reliable thermodynamic model for the solid solution. Indeed, the thermodynamic modelling of solid solutions is based on the well-known sublattice (SL) model implemented in the compound energy formalism (CEF) [24]. In this formalism, the design of a SL should result from the merging of crystal sites exhibiting comparable occupancies [25]. However, the SL models for this solution available in the literature have been built mainly on practical considerations [26] or have been based on crystal data whose reliability is questioned [27] as discussed in our previous study. Finally, it should be noted that the use of an inappropriate SL model leads inexorably to a misdescription

of the configurational entropy of mixing. It could be argued that this erroneous description can be compensated for by the use of an excess entropy term but since the latter is independent of temperature, it will only be possible to compensate for the use of an inadequate SL model at one temperature.

This paper proposes to investigate the thermodynamic stability of the $Al_{13}Fe_4$ solid solution upon substitution by Mn atoms. For this purpose, the isobaric heat capacity of the solution was measured at three different compositions from 600 K up to a temperature close to the melting temperature of the solution, with an accuracy of 95%. One of these compositions corresponds to the $Al_{13}Fe_4$ binary compound whose measured heat capacity is significantly different from other measurements available in the literature [28, 29, 30]. We show in this paper that our measurements are not only more accurate than those available in the literature but also in much better agreement with the calculations [2, 31, 32, 33] and measurements [34, 35] of the enthalpy of formation of the $Al_{13}Fe_4$ intermetallic compound available in the literature and obtained in this work. In addition, the enthalpies of formation of 8 ternary alloys with two different chemical compositions were measured by differential scanning calorimetry (DSC). New $ab-initio$ calculations of the enthalpies of formation at 0 K of the solid solution were also performed in this work. These calculations and measurements were complemented by a configurational entropy model based on the Bragg-Williams approximation [24] to forecast the thermodynamic behaviour of the solid solution with respect to both temperature and chemical composition. Note also that the site occupation factors (sof) of the structure were calculated to evaluate the ordering of the solution as a function of temperature. These last calculations allow us to determine if the new SL model we developed for the $Al_{13}Fe_4$ based solid solutions [22] is transferable to the Al-Fe-Mn ternary system.

2. Methodology

2.1. In-situ synthesis - DSC measurements

The alloys we synthesized were obtained from a mixture of pure element powders (from AEE (3N purity)) placed in a capped alumina crucible mounted on the type-S DSC plate rod of the Setaram Labsys-Evo. The compositions of the alloys were chosen to be consistent with those of the first two *end-members* i.e. $x = 2/3$ and $4/3$ in $Al_{13}Fe_{4-x}Mn_x$. A heating rate of 5 K/min was used

for the synthesis. The calibration of our equipment follows the standard methods recommended in the literature [36, 37, 38]. This measurement methodology has been described in detail in one of our previous studies [22] and the interested reader is referred to it. The samples were also analysed by X-ray diffraction (XRD) using a Empyrean 3 diffractometer developped by Malvern PanAlytical. The composition of the alloys we synthesized as well as the result of the XRD characterisation are summarised in Table 2.

2.2. Cp measurements

Isobaric heat capacity measurements were conducted on three samples synthesized $in-situ$ with different chemical compositions: the $Al_{13}Fe_4$ composition as well as the two chemical compositions detailed in section 2.1. The samples were crushed into powder in an agate crucible. A mass of 410 mg $\pm$ 20 mg of powder was packed into a capped alumina liner and enclosed in a platinum crucible. The crucible is then loaded onto the 3D-Cp sensor (pseudo Tian-Calvet sensor) of a Setaram Labsys Evo instrument. The atmosphere control procedure is similar to the one used for the $in-situ$ synthesis. The heat capacity measurement was performed in continuous mode, from 473 K to a temperature close to the melting point of the synthesised alloys (1223 K, 1150 K and 1110 K for $x = 0$, $x = 2/3$ and $x = 4/3$ in $Al_{13}Fe_{4-x}Mn_x$, respectively), with a heating rate of 5 K/min. Calibration of the 3D-Cp sensor was performed using a standard sapphire sample supplied by Setaram. This sample is in the form of a solid cylinder machined to fit the dimensions of the alumina liner. The sapphire sample is placed in the alumina liner, which in turn is placed in the platinum crucible, closed by the lids. Calibration is carried out to measure the sensitivity of the sensor continuously over the entire temperature range. For each alloy composition, this procedure was repeated three times and the data sets from these measurements were averaged. The maximum deviation between the three individual data sets did not exceed 5%. The average heat capacity was then fitted by a Maier-Kelley function [39]. It is important to note that the relative difference between the raw heat capacity values and the fitted values does not exceed 3%. This procedure was validated by the heat capacity measurements of two reference samples, aluminium powder of 3N purity (measured up to 900 K), and a solid alumina sample (measured up to 1350 K). Each individual measurement of the heat capacity of these reference samples allowed us to ensure that an accuracy higher than 95% can be achieved above 600 K. Based on these results, we believe that the nature of the samples (powder or solid) has only a marginal impact on the accuracy of the

measurement when using a 3D-Cp probe. These measurements are reported in Appendix.

2.3. DFT calculations

DFT calculations were conducted in the generalized gradient approximation (GGA) framework by means of the Perdew-Burke-Ernzerhof (PBE) exchange-correlation function [40] implemented in the VASP code [41, 42]. We used a 6 x 11 x 7 k-points grid. Projector augmented wave (PAW) pseudopotentials were applied with a cut-off energy of 600 eV. We selected potentials with 3, 8 and 13 valence electrons for Al, Fe and Mn respectively. In order to take into account the magnetic nature of Fe, our calculations were carried out in spin polarisation. Both lattice parameters and atomic positions were relaxed until the Hellman-Feynman forces were lower than 1 meV/Å. Finally, Blöchl corrections were applied in order to obtain very accurate total energy values [43]. The distribution of Mn atoms on the five non-equivalent Fe sites generates 32 *end-members* for which the total energies have been determined. The coordinates of the crystal sites of the $Al_{13}Fe_4$ structure are summarised in Table 1.

The enthalpy of formation of an ordered compound is determined by the difference between its total energy and the sum of the pure element energies that compose the compound, in their respective standard state (Al-fcc, Fe-bcc, Mn-$A12$).

The enthalpy of mixing is equal to the difference between the calculated formation enthalpy of the $Al_{13}Fe_{4-x}Mn_x$ solid solution *end-members* ($x \neq 0,\ 4$) to the composition-weighted formation enthalpies of reference compounds (*i.e.* $Al_{13}Fe_4$ and $Al_{13}Mn_4$ compounds).

2.4. Thermodynamic modelling to compute site occupancy factors

The site occupancies were calculated using the Bragg-Williams approximation [24] (*i.e.* neglecting the non-configurational entropy contributions). Considering the solid solution along the $Al_{13}Fe_4$-$Al_{13}Mn_4$ isocomposition line and considering the five Fe sites separately, the Gibbs free energy is given by:

$$G^{Al_{13}(Fe,Mn)_4}(T) = \sum_{a,b,c,d,e=\mathrm{Fe,Mn}} \left[y_a^{SL_1} y_b^{SL_2} y_c^{SL_3} y_d^{SL_4} y_e^{SL_5} \right] \cdot H_{abcde}^{Al_{13}(Fe,Mn)_4} + RT \sum_s m^{(s)} \cdot \sum_{a=\mathrm{Fe,Mn}} y_a^{(s)} \ln y_a^{(s)} \quad (1)$$

$y_b^{SL_a}$ is the sof of the element b on the a-th SL, $H_{abcde}^{for,Al_{13}Mn_4}$ is the enthalpy of formation of the considered $end-member$, R is the gas constant, m^{SL_a} is the a-th SL multiplicity.

3. Results and Discussion

3.1. Experimental investigations

Figure 1 shows the DSC signals of the $Al_{13}Fe_{4-x}Mn_x$ alloys synthesis for different values of x. The DSC signal consists of a single, particularly sharp, exothermic peak that stands out from the baseline. For the two alloys synthesised in this study, this exothermic peak extends over 12 K $\pm$ 1 K from 918 K $\pm$ 1 K, the onset of the peak is obtained at 920 K $\pm$ 1 K. No additional peaks are evidenced on the DSC signals which shows that no other reaction occurs apart from the one associated to this exothermic peak. The XRD characterisations carried out following these experiments show that our samples exhibit the crystal structure of the $Al_{13}Fe_4$ binary compound as reported in Fig. 2 and Fig. 3. The exothermic peak identified in the DSC measurements therefore corresponds to the solid solution synthesis reaction. It should be noted that the synthesis reaction of the solid solution from its pure elements is almost complete (greater than 97 wt%) as shown in Table 2, Fig. 2 and Fig. 3. For all the alloys synthesised in this study, the remaining mass corresponds to aluminium. From these experiments, the enthalpy of formation of the solid solution was determined by integrating the DSC exothermic peak between 910 K and 930 K. Note that we have subtracted the remaining mass of pure aluminium in our samples for the calculation of the formation enthalpy. The resulting formation enthalpy values are reported in Table 3 and Fig. 4. Although our measurements were not carried out under strictly isothermal conditions, it is important to note that the variation in formation enthalpy of the solid solution between 910 K and 930 K is negligible. Indeed, for a given composition, this variation corresponds to the deviation between the integral of the Neumann-Kopp rule (NKR) heat capacity [44] and the integral of the solid solution heat capacity. Based on the heat capacities measured in this study, the resulting variations in formation enthalpy are 40.3 J.mol-at $^{-1}$ and 37.6 J.mol-at $^{-1}$ for $x = 2/3$ and $x = 4/3$ in $Al_{13}Fe_{4-x}Mn_x$, respectively, *i.e.* close to 0.1% of the formation enthalpy values we obtained. Finally, it should be noted that the measurements carried out in this study were repeated four times, leading to formation enthalpy values very close to each other, as shown in Table 3. These measurements indicate that the substitution of Fe by Mn in the solid solution is associated with

a pronounced increase in the enthalpy of formation values. Note that our DFT calculations also show that the enthalpy of formation of the solid solution increases significantly upon substitution of Fe by Mn.

This same measurement methodology was presented in one of our previous study [22] and allowed us to obtain very accurate formation enthalpy values for the $Al_{13}Fe_4$ binary compound *i.e.* -26.8 kJ.mol-at $^{-1}$ *vs* -27.9 kJ.mol-at $^{-1}$ [34] and -26.2 kJ.mol-at $^{-1}$ [35]. Moreover, the measurements carried out in this paper allow us to have a precise evaluation of their accuracy. Indeed, we can notice that no stable *end-member* is found at composition $x = 2/3$ in $Al_{13}Fe_{4-x}Mn_x$. Consequently, the variation of the solid solution formation enthalpy from $x = 0$ to $x = 4/3$ in $Al_{13}Fe_{4-x}Mn_x$ is linear. The linear regression of our measurements reported in Fig. 5 shows that the formation enthalpy values we measured have a maximum deviation of 0.5 kJ.mol-at $^{-1}$, which is consistent with the deviation estimated in our previous study [22].

The heat capacity of the $Al_{13}Fe_4$ binary compound measured in this work is presented in Figure 7 and compared to the existing measurements in the literature and to the heat capacity derived of the NKR.

It should be noted firstly that the initial heat capacity value we obtained at 600 K for the $Al_{13}Fe_4$ binary compound is in good agreement with the measurements of Illekova *et al.* [28], Zienert *et al.* [29] and Rank *et al.* [30] as seen in Figure 7. On the other hand, the measurements of Zienert *et al.* and Rank *et al.* show an inflection of the heat capacity from 600 K onwards, while our measurements report on the contrary an almost linear increase, leading to significantly higher heat capacity values. These discrepancies can be explained by the methodology of the measurement employed. Indeed, the measurements available in the literature are based on standard planar DSC methods whereas it is recommended to use three-dimensional calorimetry methods (known as the Tian-Calvet method) in order to obtain accurate heat capacity measurements [45, 46]. In addition, Zienert *et al.* [29] and Illekova *et al.* [28] used standard calibration methods [36, 37, 38] whereas the Tian-Calvet rods have to be calibrated by Joule effect or with a sapphire standard which considerably reduces the error associated with the conventional calibration of planar DSC rods [46]. Furthermore, it should be noted that the calculations and measurements of enthalpy of formation available in the literature [2, 31, 32, 33, 34, 35] suggest that the heat capacity of the $Al_{13}Fe_4$ binary compound is higher than the one obtained with NKR since the enthalpy values increase between 0 K [2, 31, 32, 33, 22]

and 920-930 K [34, 35, 22]. Although the heat capacity we measured is slightly lower than the one obtained by NKR, our results still show a much better thermodynamic consistency with the data sets available in the literature. For instance, the difference between the heat capacity of the $Al_{13}Fe_4$ binary compound measured in the present work or obtained by NKR leads to a decrease of the enthalpy of formation of 0.4 kJ.mol-at $^{-1}$ between 600 K and 1323 K against a decrease of 1.6 kJ.mol-at $^{-1}$ if we consider the heat capacity measured by Zienert *et al.* [29] or Rank *et al.* [30]. Consequently, our measurements and calculations of the enthalpy of formation [22] and the heat capacity of the $Al_{13}Fe_4$ compound allow a coherent description of the energetics of this phase considering the standard errors linked to the DFT calculations of formation enthalpy using the PBE exchange-correlation functional (around 10% of relative error [47, 48]), to the measurement of the enthalpy of formation (5% of relative error [22]) and to the measurement of the heat capacity (5% of relative error).

The heat capacity of the $Al_{13}Fe_{4-x}Mn_x$ solid solution is plotted at different composition in Figure 8. This figure illustrates that the substitution of Fe by Mn in the $Al_{13}Fe_4$ structure only has a limited incidence on the heat capacity of the solid solution. Indeed, the maximum difference between the heat capacity of the $Al_{13}Fe_4$ binary compound and the solid solution composition $x = 4/3$ in $Al_{13}Fe_{4-x}Mn_x$ is less than 1 J.K^{-1}.mol-at $^{-1}$.

3.2. DFT calculations

In Table 4 are listed the composition of the ordered configurations generated for the solid solution $Al_{13}(Fe,Mn)_4$ as well as the calculated values of their enthalpies of formation. The formation enthalpy value we obtained for the $Al_{13}Fe_4$ binary compound (-31.335 kJ.mol-at $^{-1}$) is relatively close to those available in the literature [2, 31, 32, 33], ranging from -33.481 kJ.mol-at $^{-1}$ to -30.876 kJ.mol-at $^{-1}$. It should be noted that our calculations performed in spin polarisation showed that the $Al_{13}Fe_4$ phase is non-magnetic, in good agreement with the literature data [2]. Indeed, Fang *et al.* have shown that only an increase in Fe content (by substituting Al with Fe) allows the emergence of a ferromagnetic or antiferromagnetic ordering. Thus, our calculations are in good agreement with the investigations of Fang *et al.* since all the *end-members* of the $Al_{13}(Fe,Mn)_4$ phase are non-magnetic. To our knowledge, no other thermodynamic parameters of any *end-member* we studied in this paper have been published in the literature. The formation enthalpy of the solid solution *end-members* are summarised in Fig. 4. This figure clearly illustrates the

strong thermodynamic destabilisation that occurs within the solid solution when Fe is replaced by Mn. Furthermore, these results can be compared to our DSC measurements carried out at 920 K showing that the thermodynamic destabilisation of the solid solution induced by Mn substitution is also observed at higher temperatures as reported in Fig. 4.

The DFT calculations presented in the Table 4 were also used considering the $Al_{13}Fe_4$ and $Al_{13}Mn_4$ binary compounds as reference states in order to deduce the 0 K enthalpy of mixing of the solution as plotted in Fig. 6. In this figure, the distribution of Mn atoms on the Fe sites appears to be chemically ordered. The sequence of Mn substitution when changing composition from $Al_{13}Fe_4$ to $Al_{13}Mn_4$ is the following: site Fe(5), site Fe(3), site Fe(4), site Fe(2) and site Fe(1) (site notation is taken from [49]). Pang *et. al* [4] also indicated that Mn more favorably occupies site Fe(5) thanks to calculations simulating single-atom substitution. Our study, on the other hand, employs a methodology that allows the examination of all chemical compositions. Note that the enthalpy of mixing of the solid solution shown in Fig. 6 is only weakly exothermic (minimum of mixing enthalpy close to -0.6 kJ/mol) reflecting its weak ordering.

3.3. Thermodynamic modelling and site occupancy factors calculations

The thermodynamic modelling of the solid solution was achieved considering the enthalpies of formation calculated and measured in this study, the formation enthalpy of the $Al_{13}Fe_4$ binary compound measured at 920 K in our previous study as well as measurements available in the literature [34, 35].

The thermodynamic assessment of the $Al_{13}(Fe,Mn)_4$ solid solution was performed using the Calphad approach. In a first step, the enthalpies of formation of the *end-members* of the solid solution were fixed to the values we calculated by DFT. The heat capacity of the *end-members* of the solid solution were initially set to the values we measured. Since our measurements showed that the heat capacity value of the solid solution does not change significantly with chemical composition, all *end-members* of the solid solution were described with the heat capacity of the $Al_{13}Fe_4$ binary compound. In a second step, the thermodynamic parameters of the *end-members* were optimised taking into account the enthalpies of formation that we measured in this study. No interaction parameters were used to model this solid solution. The Gibbs energy functions we evaluated represent the best compromise between all the measurements and calculations we performed in this study. All the data considered for this optimisation are accurately modelled (relative deviation less than the

error bars of measurements and calculations). The Gibbs free energy function of each *end-member* is summarised in the table 5. This thermodynamic modelling was then used to calculate the Fe sof of the solid solution structure.

The Fe sof calculated at 300 K are plotted in Fig. 9. This figure highlights that the Fe sites are not equivalent at this temperature since the sof values are very different from each other, except for the sites Fe(3) and Fe(4). The chemical ordering of the solution thus consists in the preferential substitution of Mn on site Fe(5), followed by sites Fe(3), Fe(4), Fe(2), Fe(1), which is consistent with our $ab-initio$ calculations. Furthermore, by restricting the investigation of the solid solution crystal chemistry to its homogeneity range (indicated in blue in Fig. 9), it can be assumed that both sites Fe(2) and Fe(1) are similar with respect to Mn substitution. The Fe sof were also calculated at 920 K in Fig. 10 as well as 1173 K in Fig. 11, temperature for which the stability range of the solid solution is particularly wide [23]. From these two figures, it appears that Mn site occupancies tend towards ideal values for all Fe sites as the temperature increases $i\ e.$ sof close to the mole fraction. The Fe sof of the solid solution allows us to calculate its configurational entropy as presented in Fig. 12: While a partial ordering can be noticed at 300 K, the solution is almost ideally disordered at 920 K and 1173 K.

4. Conclusion

In this paper, the thermodynamic stability of the $Al_{13}Fe_4$ solid solution was investigated along with its crystal chemistry in the entire chemical composition range of the Al-Fe-Mn ternary system *i.e.* mimicking the complete substitution of Fe atoms by Mn, and from room temperature up to the melting temperature of the solid solution.

To do so, the enthalpy of formation of the *end-members* of the solution were calculated by DFT at 0 K. In addition, the enthalpy of formation of the solid solution has been measured by *in-situ* synthesis in a DSC. Our calculations and experiments show that the substitution of Mn on the Fe sites leads to a thermodynamic destabilisation of the solid solution. Moroever, the isobaric heat capacity of the solid solution was measured from 600 K up to the melting temperature of the solid solution, with an accuracy of 95%. Note that the heat capacity measurement performed on the $Al_{13}Fe_4$ binary compound is both more accurate than those available in the literature but also in

better agreement with other thermodynamic data available for this phase. By combining these new data with a configurational entropy model based on the Bragg-Williams approximation [24], we calculated the Fe sof of the $Al_{13}Fe_4$ structure, in the whole chemical composition and temperature range of stability.

Our calculations show that the solid solution is chemically ordered at low temperature (below 300 K). In contrast, above 920 K, the quasi ideal configurational entropy of mixing is responsible for the stability of the solution. Thus, the sublattice model we designed for the $Al_{13}Fe_4$ solid solutions in the Al-Fe-Co, Al-Fe-Cr and Al-Fe-Ni ternary systems [22] is ideally suited to describe the solid solution in the Al-Fe-Mn ternary system. This model relies on two sublattices (one sublattice relative to the Fe sites, the second sublattice merging all the Al sites) with mixing on each SL.

5. Acknowledgement

This work was financially supported by the Professor Harvey Discovery Grant (RGPIN-2017-06168) (NSERC)

Funding support was obtained through the Alliance grant (ALLRP 560998 - 20).

Compute Quebec and Compute Canada are thanked for supplying the intensive calculation tools.

XRD characterizations were kindly provided by Dr. Maris and Dr. Chartrand.

References

[1] A. Dinsdale, C. Fang, Z. Que, Z. Fan, JOM 71 (2019) 1731–1736.

[2] C. Fang, A. Dinsdale, Z. Que, Z. Fan, Journal of Physics: Materials 2 (2019) 015004.

[3] C. Fang, Z. Que, A. Dinsdale, Z. Fan, Intermetallics 126 (2020) 106939.

[4] N. Pang, Z. Shi, C. Wang, N. Li, Y. Lin, Materials 14 (2021) 768.

[5] J. Mathew, G. Remy, M. A. Williams, F. Tang, P. Srirangam, JOM 71 (2019) 4362–4369.

[6] F. Yan, S. Kumar, B. Mckay, K. O'Reilly, International Journal of Cast Metals Research 27 (2014) 202–206.

[7] J. Wang, Y. Zhou, M. He, L. Xu, P. Wangyang, Journal of Alloys and Compounds 737 (2018) 14–20.

[8] A. Samuel, G. Garza-Elizondo, H. Doty, F. Samuel, Materials & Design 80 (2015) 99–108.

[9] T. Yamada, T. Kojima, E. Abe, S. Kameoka, Y. Murakami, P. Gille, A. P. Tsai, Journal of the American Chemical Society 140 (2018) 3838–3841.

[10] P. Gille, B. Bauer, Crystal Research and Technology: Journal of Experimental and Industrial Crystallography 43 (2008) 1161–1167.

[11] J. Cabrera-Trujillo, J. Moran-Lopez, V. Kumar, Journal of Physics: Condensed Matter 5 (1993) A399.

[12] S. Hirt, F. Yuan, Y. Mozharivskyj, H. Hillebrecht, Inorganic Chemistry 55 (2016) 9677–9684.

[13] D. K. Mann, Y. Wang, J. D. Marks, G. F. Strouse, M. Shatruk, Inorganic Chemistry 59 (2020) 12625–12631.

[14] L. Zhu, S. Soto-Medina, R. G. Hennig, M. V. Manuel, Journal of Alloys and Compounds 815 (2020) 152110.

[15] B. Bauer, P. Gille, Zeitschrift für anorganische und allgemeine Chemie 637 (2011) 2052–2058.

[16] L. Zhang, Y. Du, Calphad 31 (2007) 529–540.

[17] L. Zhang, Y. Du, H. Xu, C. Tang, H. Chen, W. Zhang, Journal of alloys and compounds 454 (2008) 129–135.

[18] B. Grushko, Journal of Alloys and Compounds 829 (2020) 154444.

[19] V. Witusiewicz, A. Bondar, U. Hecht, V. Voblikov, N. Tsyganenko, O. Fomichov, M. Karpets, V. Petyukh, T. Y. Velikanova, Journal of Materials Science 48 (2013) 377–412.

[20] T. Yanson, N. Manyako, O. Bodak, R. Cêrny, R. Gladyshevskii, K. Yvon, Journal of Alloys and Compounds 219 (1995) 135–138.

[21] I. Lee, K. Han, I. Ohnuma, R. Kainuma, Journal of Alloys and Compounds 854 (2021) 157163.

[22] P. Lafaye, K. Oishi, M. Bourdon, J.-P. Harvey, Journal of Alloys and Compounds (2022) Available online 8 June 2022, 165779, In Press.

[23] S. Balanetskyy, D. Pavlyuchkov, T. Velikanova, B. Grushko, Journal of Alloys and Compounds 619 (2015) 211–220.

[24] M. Hillert, Journal of Alloys and Compounds 320 (2001) 161–176.

[25] H. Lukas, S. G. Fries, B. Sundman, Computational thermodynamics: the Calphad method, Cambridge university press, 2007.

[26] P. Wang, W. Xiong, U. R. Kattner, C. E. Campbell, E. A. Lass, O. Y. Kontsevoi, G. B. Olson, Calphad 59 (2017) 112–130.

[27] B. Sundman, I. Ohnuma, N. Dupin, U. R. Kattner, S. G. Fries, Acta Materialia 57 (2009) 2896–2908.

[28] E. Illeková, J.-C. Gachon, J.-J. Kuntz, in: Thermophysics 2002. Meeting of the Thermophysical Society Working Group of the Slovak Physical Society, October 24-25, 2002, Kočovce, Slovakia, pp. 71–76.

[29] T. Zienert, A. Leineweber, O. Fabrichnaya, Journal of Alloys and Compounds 725 (2017) 848–859.

[30] M. Rank, P. Gotcu, P. Franke, H. J. Seifert, Intermetallics 94 (2018) 73–82.

[31] M. Mihalkovič, M. Widom, Physical Review B 85 (2012) 014113.

[32] A. Van der Kraan, K. Buschow, Physica B+ C 138 (1986) 55–62.

[33] T. Klaver, G. Madsen, R. Drautz, Intermetallics 31 (2012) 137–144.

[34] W. Biltz, Zeitschrift Fuer Metallkunde 29 (1937) 72–79.

[35] O. Kubaschewski, W. Dench, Acta Metallurgica 3 (1955) 339–346.

[36] ASTM-E967-18, ASTM International, West Conshohocken, PA (2018).

[37] ASTM-E968-02, ASTM International, West Conshohocken, PA (2014).

[38] G. Della Gatta, M. J. Richardson, S. M. Sarge, S. Stølen, Pure and applied chemistry 78 (2006) 1455–1476.

[39] C. G. Maier, K. Kelley, Journal of the American chemical society 54 (1932) 3243–3246.

[40] J. P. Perdew, K. Burke, M. Ernzerhof, Physical review letters 77 (1996) 3865.

[41] G. Kresse, J. Furthmüller, Physical review B 54 (1996) 11169.

[42] G. Kresse, D. Joubert, Physical review b 59 (1999) 1758.

[43] P. E. Blöchl, Physical review B 50 (1994) 17953.

[44] H. Kopp, Philosophical Transactions of the Royal Society of London (1865) 71–202.

[45] E. Calvet, H. Prat, Récents progrès en microcalorimétrie, volume 6, Dunod, 1958.

[46] C. N. de Castro, M. Lourenço, M. Sampaio, Thermochimica Acta 347 (2000) 85–91.

[47] K. Lejaeghere, V. Van Speybroeck, G. Van Oost, S. Cottenier, Critical reviews in solid state and materials sciences 39 (2014) 1–24.

[48] S. Lany, Physical Review B 78 (2008) 245207.

[49] J. Grin, U. Burkhardt, M. Ellner, K. Peters, Zeitschrift für Kristallographie-Crystalline Materials 209 (1994) 479–487.

6. Table caption

Table 1: Crystal structure of the $Al_{13}Fe_4$ phase according to Grin *et al.* [49].

Site	**Wyckoff position**	**x**	**y**	**z**
Fe(1)	$4i$	0.0851	0	0.3821
Fe(2)	$4i$	0.4018	0	0.6234
Fe(3)	$4i$	0.0906	0	0.9889
Fe(4)	$4i$	0.4031	0	0.9859
Fe(5)	$8j$	0.3195	0.2938	0.2777
Al(1)	$4i$	0.0649	0	0.1743
Al(2)	$4i$	0.3232	0	0.2819
Al(3)	$4i$	0.2377	0	0.5349
Al(4)	$4i$	0.0736	0	0.5803
Al(5)	$4i$	0.2406	0	0.9608
Al(6)	$4i$	0.4792	0	0.8288
Al(7)	$2d$	0.5	0	0.5
Al(8)	$4i$	0.3057	0	0.7728
Al(9)	$4i$	0.087	0	0.7885
Al(10)	$8j$	0.185	0.2168	0.1106
Al(11)	$8j$	0.3677	0.2113	0.1097
Al(12)	$8j$	0.1783	0.221	0.3346
Al(13)	$8j$	0.4916	0.2334	0.3296
Al(14)	$8j$	0.3634	0.2188	0.4786
Al(15)	$4g$	0	0.2496	0

Table 2: Chemical composition of the synthesized alloys and XRD analysis.

Sample	**Chemical composition**	**Space group**	**Synthesis wt.%**	**Lattice parameters Å and °**			
	x (in $Al_{13}Fe_{4-x}Mn_x$)			a	b	c	β
1	2/3	$C2/m$	97.2	15.5448(6)	8.0578(1)	12.4763(2)	107.6952(3)
2	4/3	$C2/m$	98.1	15.6227(7)	8.0297(4)	12.4874(3)	107.6640(1)

Table 3: DSC measured enthalpies of formation (ΔH_f) of the $Al_{13}(Fe,Mn)_4$ solid solution. Reference Al (fcc), Fe (bcc) and Mn ($A12$).

Composition x (in $Al_{13}Fe_{4-x}Mn_x$)	ΔH_f **kJ.mol-at** $^{-1}$					**Ref.**
	measure 1	measure 2	measure 3	measure 4	**Average**	
2/3	-23.38	-24.64	-23.58	-24.57	**-24.04**	This work
4/3	-22.72	-22.65	-22.67	-23.01	**-22.76**	This work

Table 4: DFT calculated total energy (E_{tot}) and enthalpy of formation (ΔH_f) of the $Al_{13}(Fe,Mn)_4$ solid solution *end-members*. Sites notation are taken from [49]. Reference Al (fcc), Fe (bcc) and Mn ($A12$).

Site multiplicity					E_{tot} **eV**	ΔH_f **kJ.mol-at** $^{-1}$
Fe(1) 4	**Fe(2) 4**	**Fe(3) 4**	**Fe(4) 4**	**Fe(5) 8**		
Fe	Fe	Fe	Fe	Fe	-523.519	-31.335
Mn	Mn	Mn	Mn	Mn	-531.091	-21.849
Mn	Fe	Fe	Fe	Fe	-524.422	-29.409
Fe	Mn	Fe	Fe	Fe	-524.545	-29.526
Fe	Fe	Mn	Fe	Fe	-524.878	-29.841
Fe	Fe	Fe	Mn	Fe	-524.748	-29.718
Mn	Mn	Fe	Fe	Fe	-525.442	-27.611
Mn	Fe	Mn	Fe	Fe	-525.668	-27.824
Mn	Fe	Fe	Mn	Fe	-525.772	-27.923
Fe	Fe	Fe	Fe	Mn	-526.605	-28.711
Fe	Mn	Mn	Fe	Fe	-526.010	-28.148
Fe	Mn	Fe	Mn	Fe	-525.729	-27.882
Fe	Fe	Mn	Mn	Fe	-526.225	-28.352
Mn	Fe	Fe	Fe	Mn	-527.366	-26.650
Mn	Mn	Mn	Fe	Fe	-526.807	-26.121
Fe	Mn	Fe	Fe	Mn	-527.639	-26.909
Mn	Mn	Fe	Mn	Fe	-526.738	-26.056
Fe	Fe	Mn	Fe	Mn	-527.822	-27.082
Mn	Fe	Mn	Mn	Fe	-527.066	-26.366
Fe	Fe	Fe	Mn	Mn	-527.788	-27.050
Fe	Mn	Mn	Mn	Fe	-527.222	-26.514
Mn	Mn	Fe	Fe	Mn	-528.564	-25.003
Mn	Fe	Mn	Fe	Mn	-528.520	-24.961
Fe	Mn	Mn	Fe	Mn	-528.939	-25.357
Mn	Fe	Fe	Mn	Mn	-528.655	-25.089
Mn	Mn	Mn	Mn	Fe	-528.134	-24.597
Fe	Mn	Fe	Mn	Mn	-528.748	-25.177
Fe	Fe	Mn	Mn	Mn	-529.041	-25.455
Mn	Mn	Mn	Fe	Mn	-529.799	-23.407
Mn	Mn	Fe	Mn	Mn	-529.791	-23.400
Mn	Fe	Mn	Mn	Mn	-529.876	-23.480
Fe	Mn	Mn	Mn	Mn	-530.074	-23.668

Table 5: Thermodynamic parameters of the $Al_{13}(Fe,Mn)_4$ solid solution

Site multiplicity						**Gibbs free energy (J/mol)**				
Al(1-15) 78	**Fe(1) 4**	**Fe(2) 4**	**Fe(3) 4**	**Fe(4) 4**	**Fe(5) 8**	10^6	10^4T	$10^3TLn(T)$	T^2	10^7T^{-1}
Al	Fe	Fe	Fe	Fe	Fe	-3.7182	1.2246	-2.219	-0.5049	1.5610
Al	Mn	Mn	Mn	Mn	Mn	-3.0398	1.2357	-2.219	-0.5049	1.5610
Al	Mn	Fe	Fe	Fe	Fe	-3.8109	1.2264	-2.219	-0.5049	1.5610
Al	Fe	Mn	Fe	Fe	Fe	-3.8228	1.2264	-2.219	-0.5049	1.5610
Al	Fe	Fe	Mn	Fe	Fe	-3.8549	1.2264	-2.219	-0.5049	1.5610
Al	Fe	Fe	Fe	Mn	Fe	-3.6275	1.2264	-2.219	-0.5049	1.5610
Al	Mn	Mn	Fe	Fe	Fe	-3.3892	1.2283	-2.219	-0.5049	1.5610
Al	Mn	Fe	Mn	Fe	Fe	-3.6492	1.2283	-2.219	-0.5049	1.5610
Al	Mn	Fe	Fe	Mn	Fe	-3.6593	1.2283	-2.219	-0.5049	1.5610
Al	Fe	Fe	Fe	Fe	Mn	-3.7397	1.2283	-2.219	-0.5049	1.5610
Al	Fe	Mn	Mn	Fe	Fe	-3.6822	1.2283	-2.219	-0.5049	1.5610
Al	Fe	Mn	Fe	Mn	Fe	-3.6551	1.2283	-2.219	-0.5049	1.5610
Al	Fe	Fe	Mn	Mn	Fe	-3.7031	1.2283	-2.219	-0.5049	1.5610
Al	Mn	Fe	Fe	Fe	Mn	-3.5295	1.2301	-2.219	-0.5049	1.5610
Al	Mn	Mn	Mn	Fe	Fe	-3.4755	1.2301	-2.219	-0.5049	1.5610
Al	Fe	Mn	Fe	Fe	Mn	-3.5559	1.2301	-2.219	-0.5049	1.5610
Al	Mn	Mn	Fe	Mn	Fe	-3.4689	1.2301	-2.219	-0.5049	1.5610
Al	Fe	Fe	Mn	Fe	Mn	-3.5735	1.2301	-2.219	-0.5049	1.5610
Al	Mn	Fe	Mn	Mn	Fe	-3.5005	1.2301	-2.219	-0.5049	1.5610
Al	Fe	Fe	Fe	Mn	Mn	-3.5703	1.2301	-2.219	-0.5049	1.5610
Al	Fe	Mn	Mn	Mn	Fe	-3.5156	1.2301	-2.219	-0.5049	1.5610
Al	Mn	Mn	Fe	Fe	Mn	-3.3615	1.2320	-2.219	-0.5049	1.5610
Al	Mn	Fe	Mn	Fe	Mn	-3.3572	1.2320	-2.219	-0.5049	1.5610
Al	Fe	Mn	Mn	Fe	Mn	-3.3976	1.2320	-2.219	-0.5049	1.5610
Al	Mn	Fe	Fe	Mn	Mn	-3.3702	1.2320	-2.219	-0.5049	1.5610
Al	Mn	Mn	Mn	Mn	Fe	-3.3200	1.2320	-2.219	-0.5049	1.5610
Al	Fe	Mn	Fe	Mn	Mn	-3.3792	1.2320	-2.219	-0.5049	1.5610
Al	Fe	Fe	Mn	Mn	Mn	-3.4076	1.2320	-2.219	-0.5049	1.5610
Al	Mn	Mn	Mn	Fe	Mn	-3.1987	1.2384	-2.219	-0.5049	1.5610
Al	Mn	Mn	Fe	Mn	Mn	-3.1980	1.2385	-2.219	-0.5049	1.5610
Al	Mn	Fe	Mn	Mn	Mn	-3.2061	1.2386	-2.219	-0.5049	1.5610
Al	Fe	Mn	Mn	Mn	Mn	-3.2253	1.2387	-2.219	-0.5049	1.5610

7. Figure caption

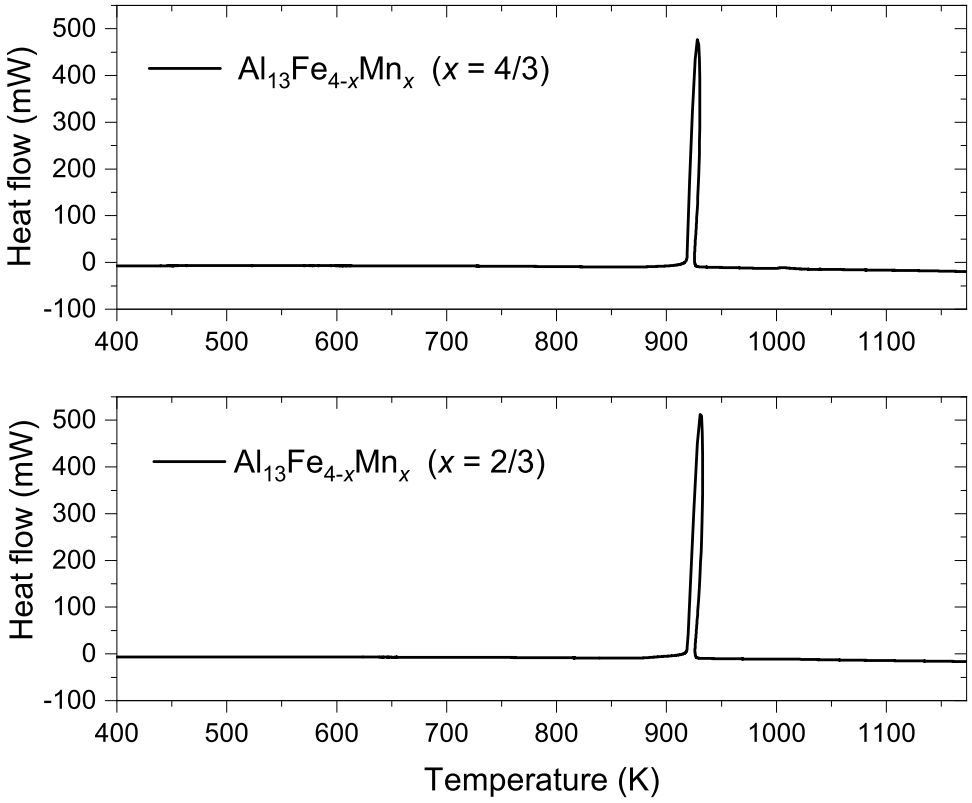

Figure 1: DSC signal resulting from the synthesis of the $Al_{13}Fe_{4-x}Mn_x$ alloys ($x = 2/3$ and $4/3$). Reference Al (fcc), Fe (bcc) and Mn ($A12$).

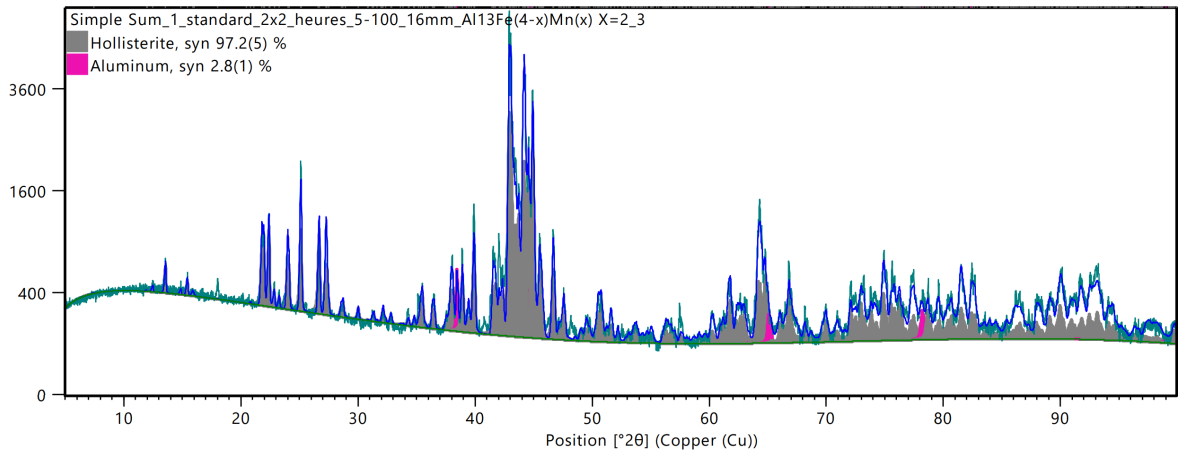

Figure 2: Rietveld refinement of the $Al_{13}Fe_{4-x}Mn_x$ alloys ($x = 2/3$). Experimental pattern is shown in blue. The evaluation of phase proportion is shown in grey and pink.

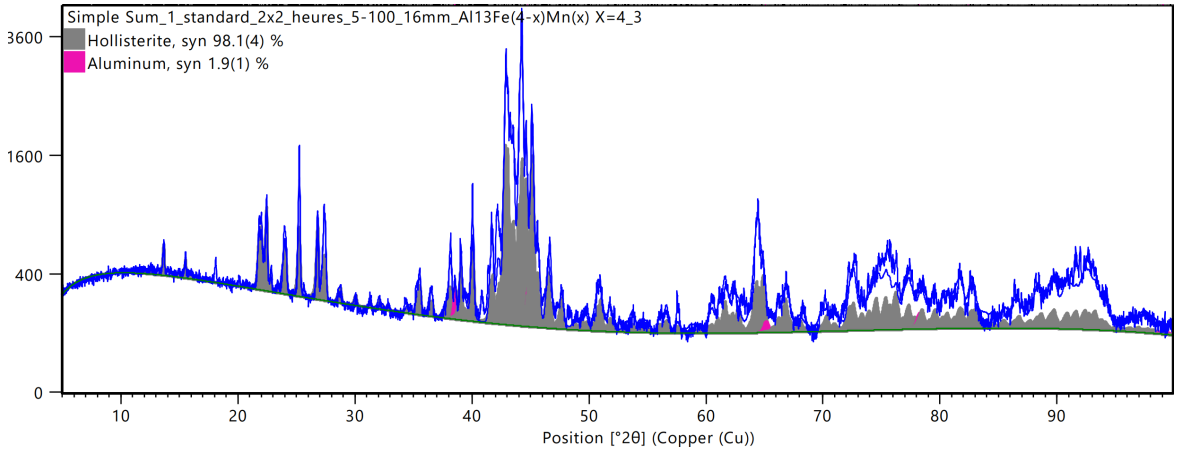

Figure 3: Rietveld refinement of the $Al_{13}Fe_{4-x}Mn_x$ alloys ($x = 4/3$). Experimental pattern is shown in blue. The evaluation of phase proportion is shown in grey and pink.

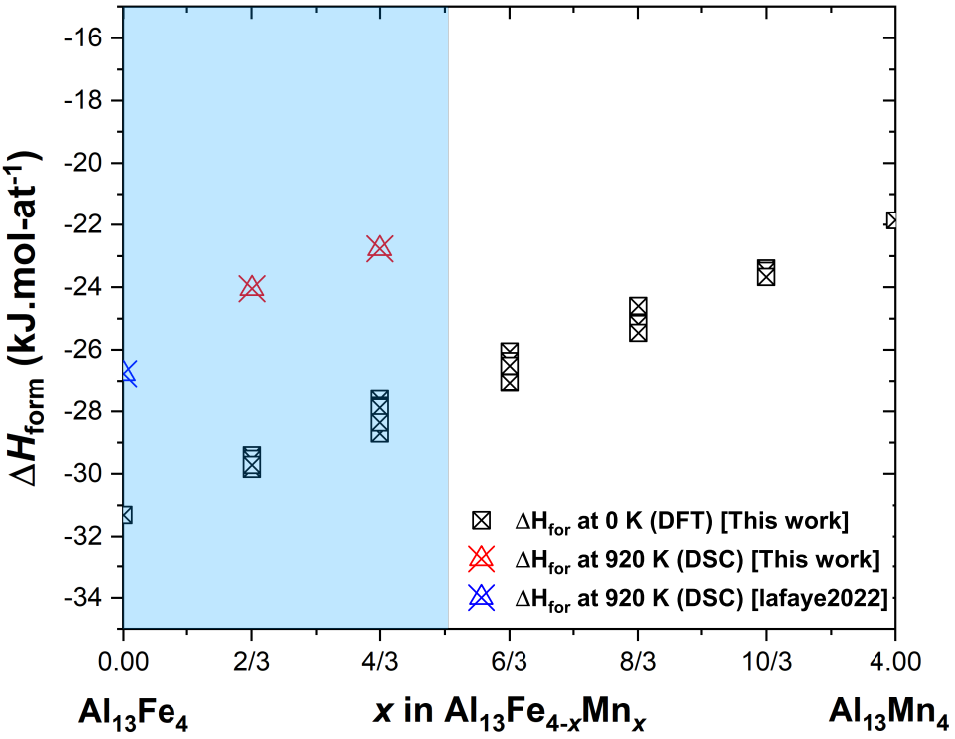

Figure 4: Enthalpies of formation of the $Al_{13}Fe_{4-x}Mn_x$ alloys (x = 0, 2/3 and 4/3) measured in this framework and from a previous study [22] together with the enthalpies of formation of the solid solution *end-members* calculated at 0 K by DFT. Reference Al (fcc), Fe (bcc) and Mn ($A12$). The ternary extension of the solid solution is shaded in blue [23].

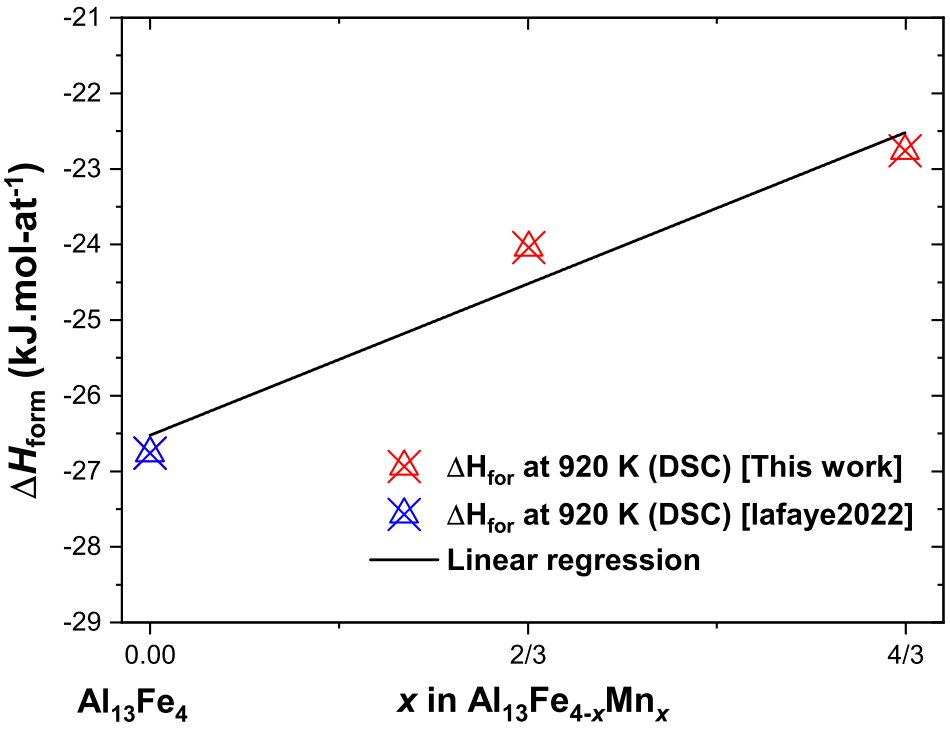

Figure 5: Linear regression of DSC measurements carried out at 920 K in this study or from our previous work [22]. Reference Al (fcc), Fe (bcc) and Mn ($A12$).

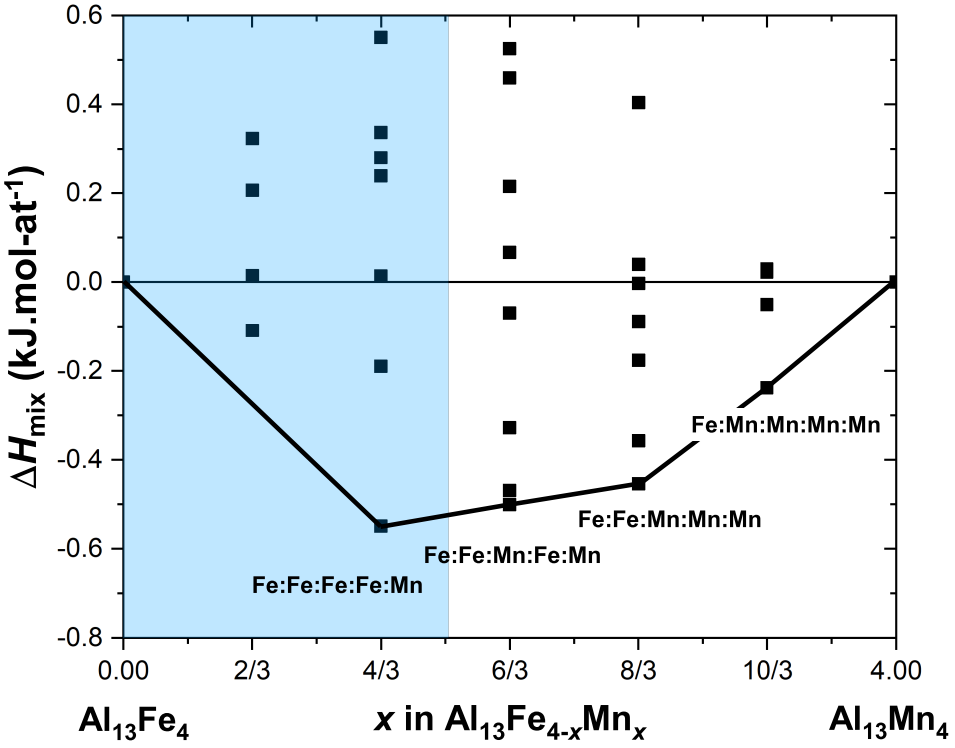

Figure 6: Calculated enthalpy of mixing of the $Al_{13}(Fe,Mn)_4$ solid solution at 0 K. The $ground-state$ configurations are reported (sites notation is taken from [49]). Reference $Al_{13}Fe_4$ and $Al_{13}Mn_4$ intermetallic compounds. The ternary extension of the solid solution is shaded in blue [23].

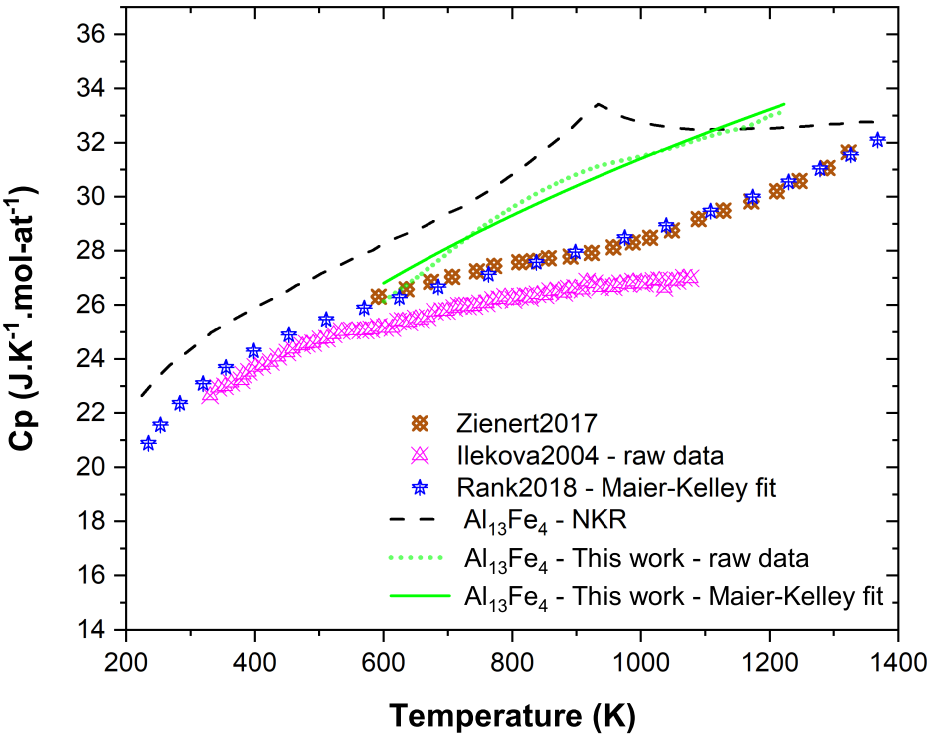

Figure 7: Isobaric heat capacity of the $Al_{13}Fe_4$ binary compound measured in the present work compared to the isobaric heat capacity derived from the NKR and available in the literature [28, 29, 30].

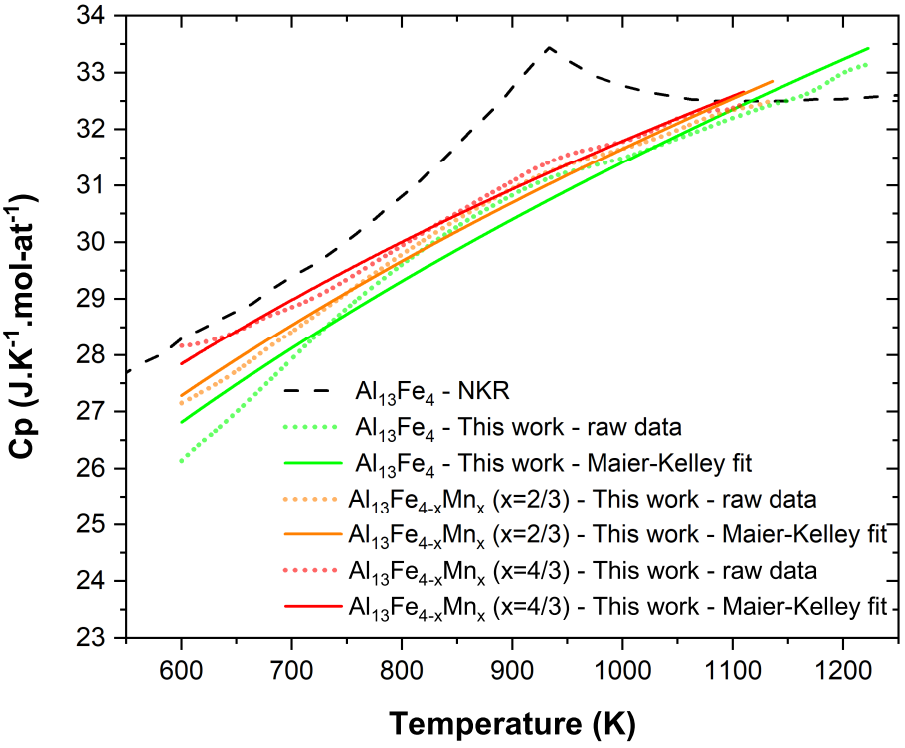

Figure 8: Isobaric heat capacity of the $Al_{13}(Fe,Mn)_4$ solid solution compared to isobaric heat capacity of the $Al_{13}Fe_4$ binary compound derived from the NKR.

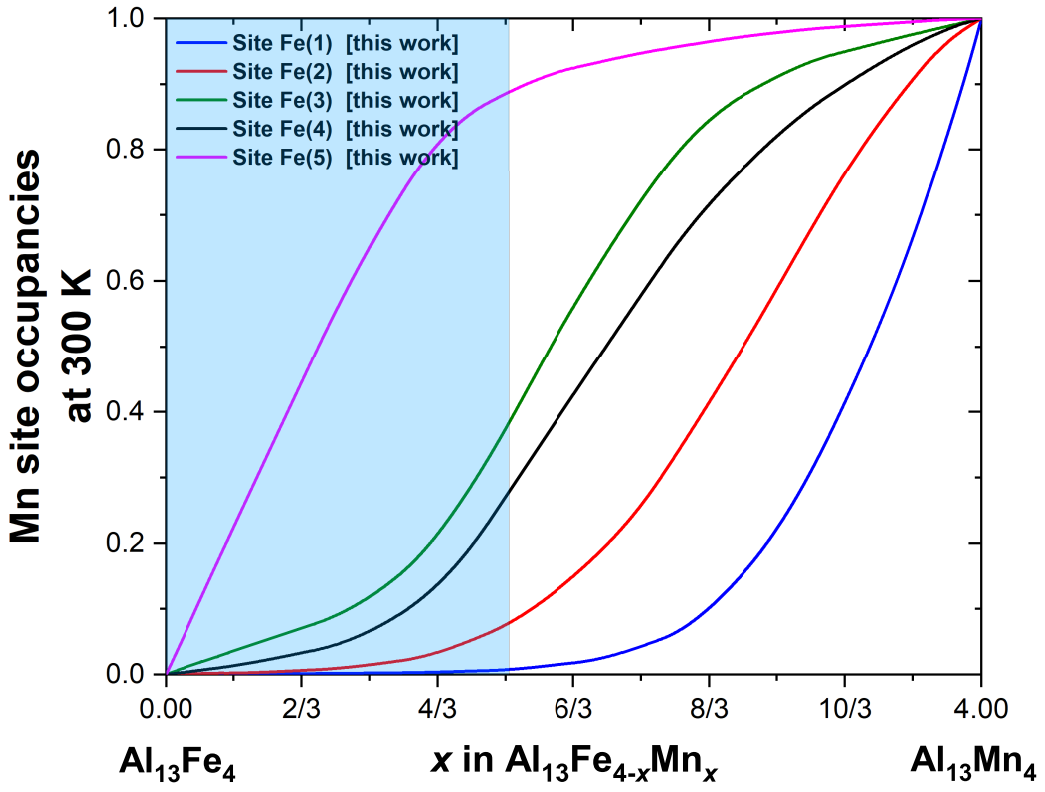

Figure 9: Site occupancy factors computed at 300 K (sites notation is taken from [49]). The ternary extension of the solid solution is shaded in blue [23].

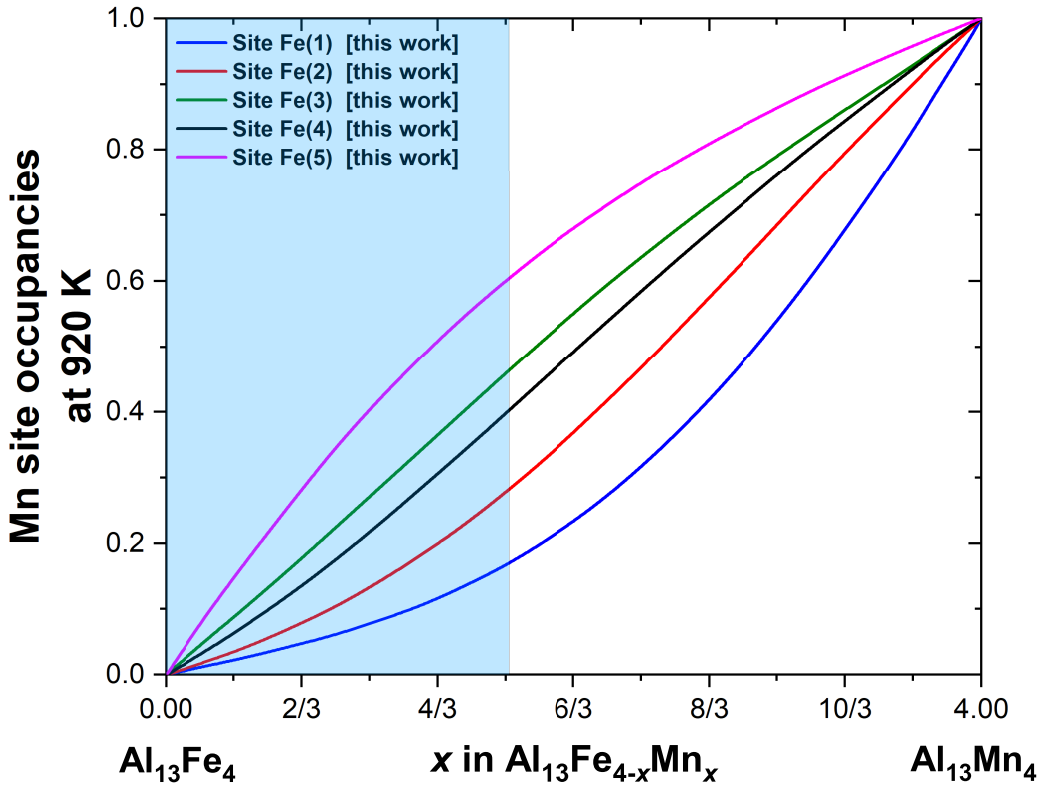

Figure 10: Site occupancy factors computed at 920 K (sites notation is taken from [49]). The ternary extension of the solid solution is shaded in blue [23].

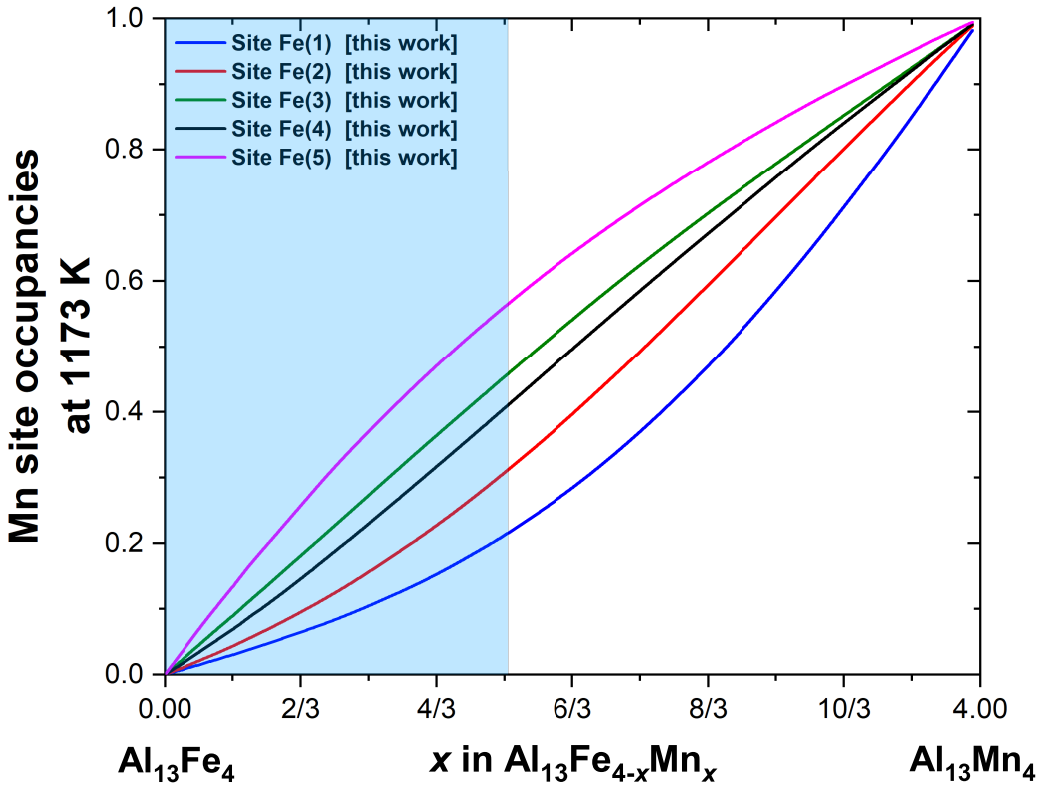

Figure 11: Site occupancy factors computed at 1173 K (sites notation is taken from [49]). The ternary extension of the solid solution is shaded in blue [23].

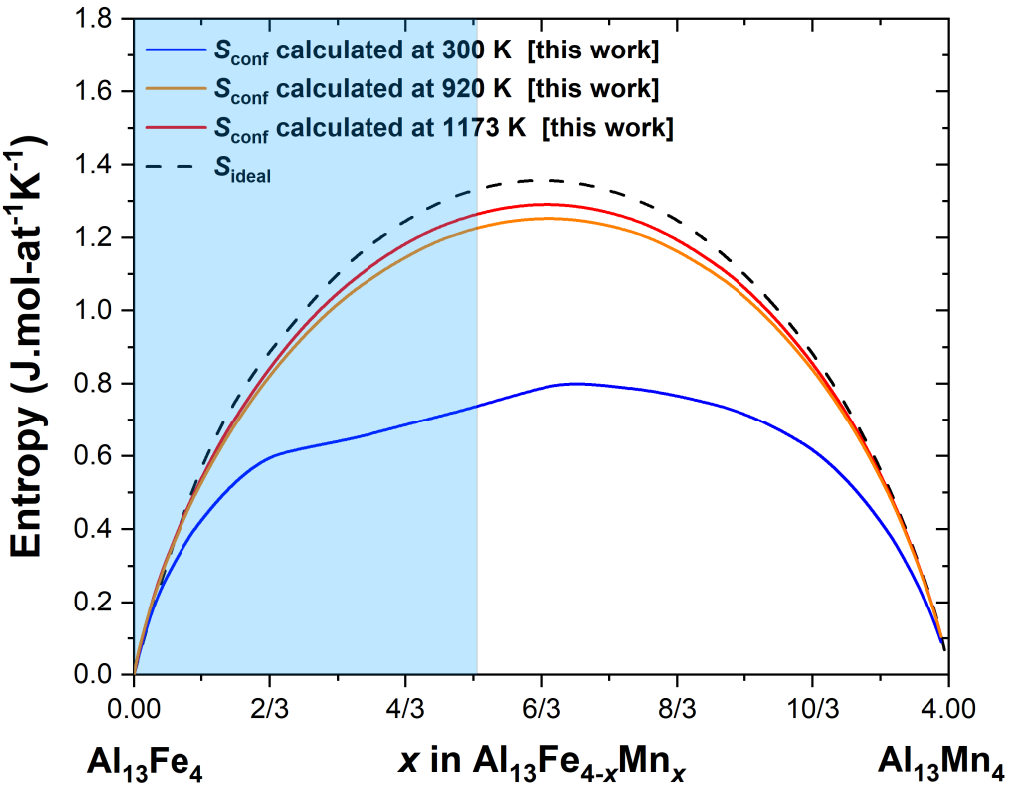

Figure 12: Configurationnal entropy (S_{conf}) calculated at 300 K, 920 K and 1173 K together with the ideal configurationnal entropy of mixing ((S_{ideal})). The ternary extension of the solid solution is shaded in blue [23].

8. Appendix

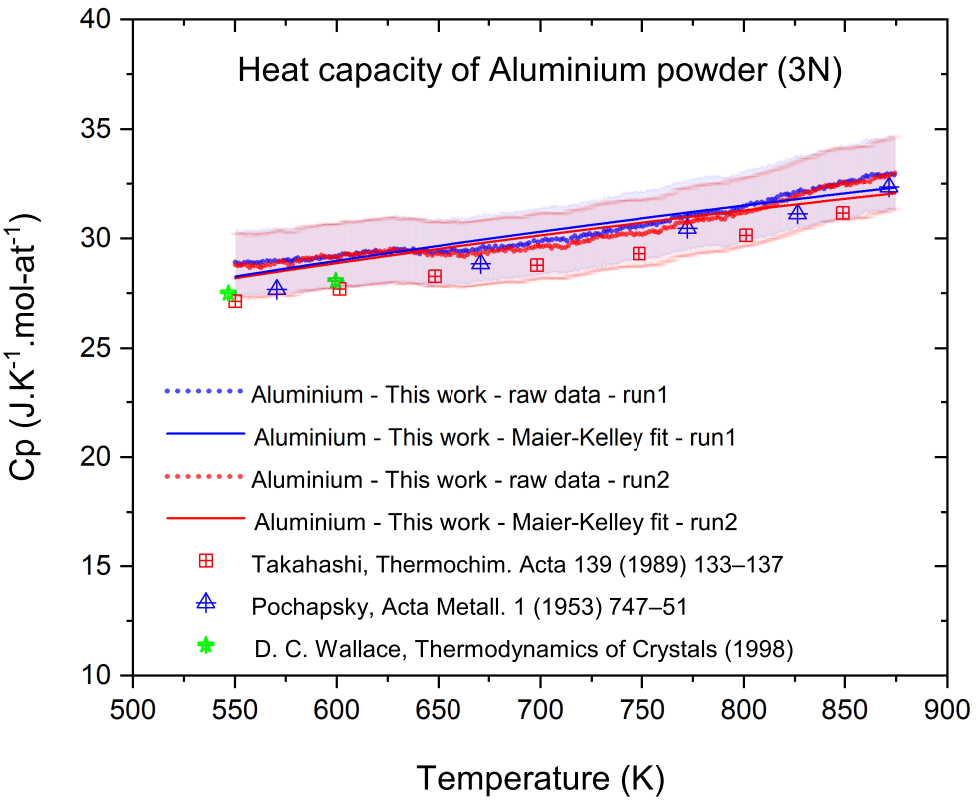

Figure 13: Heat capacity of 3N Aluminium powder measured in this work. The 5% error bars are shaded in red for run 1 and in blue for run 2.

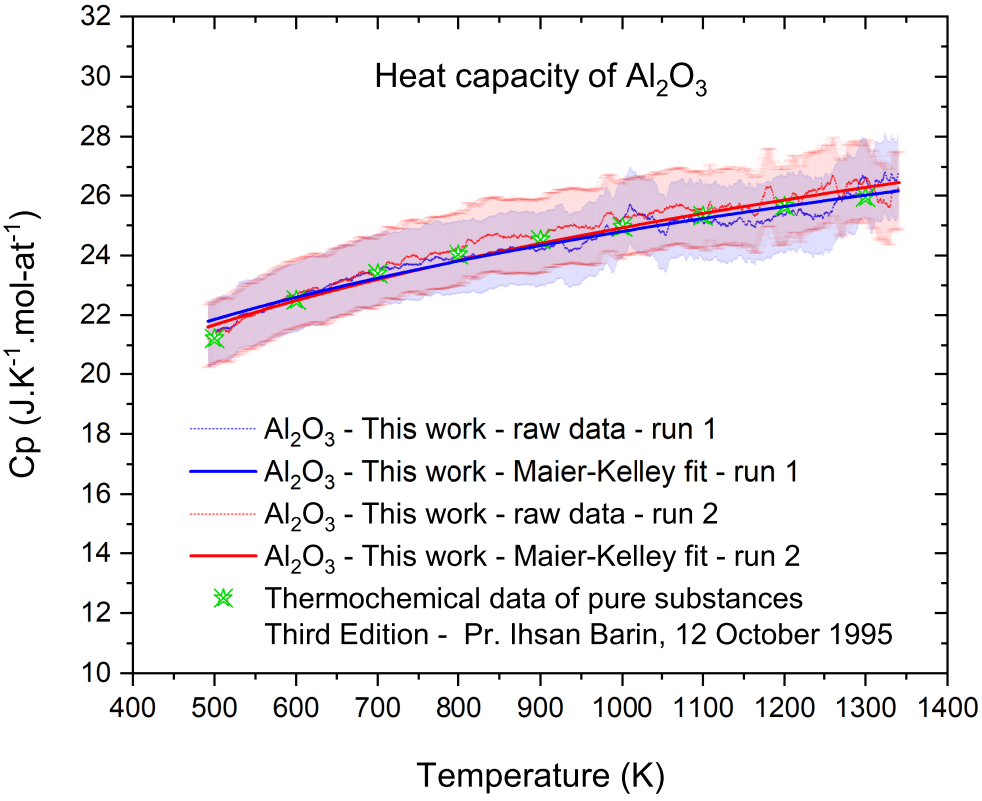

Figure 14: Heat capacity of Al_2O_3 measured in this work. The 5% error bars are shaded in red for run 1 and in blue for run 2.